MICROFLUIDIC GENERATION OF MULTICELLULAR SPHEROIDS FOR LIFE SCIENCE APPLICATIONS

Christoph Eilenberger

Harvard Medical School

Boston, MA, USA

Supervisor: Univ.Prof.Dr. Peter Ertl

Co-supervisor: Dr. Taru Muranen

Duration: 01.04.2021 – 31.08.202

TABLE OF CONTENTS

1 Background 6

1.1 The interplay of the extracellular matrix and anti-cancer drug resistance 6

1.2 Breast cancer progression and biomechanical properties 7

1.3 Three-dimensional (3D) cell models for cancer research 9

1.4 Microfluidic tumor-on-a-chip models 11

2 Aims of the project 13

3 Materials and Methods 14

3.1 Mold fabrication 14

3.2 Chip fabrication 14

3.3 Chip preparation 14

3.4 Cell culture 15

3.5 Patient-derived organoid loading 16

3.6 Green-fluorescent protein transfection 17

3.7 proliferation assay 18

3.8 Immunohistochemistry 19

3.9 Image acquisition 19

3.10 Image analysis 19

3.11 Statistical Analysis 20

4 Results 21

4.1 Microfluidic microarray concept for the generation, culture, and analysis of patient-derived breast cancer organoids 21

4.2 Optimization of the patient-derived organoid seeding protocol 22

4.3 Tumor microenvironment stiffness modulation on-chip 23

4.4 Time-resolved multi-tumor tissue growth monitoring on-chip 25

4.5 Optimization of proliferation marker staining protocols 26

4.6 Establishment of breast cancer co-culture model on-chip 27

5 Discussion *29*

6 References *31*

LIST OF FIGURES

Figure 1: Molecular subtypes of breast cancer. From biorender.com. 8
Figure 2: Overview of *in vitro* models for studying breast cancer physiopathology and for drug screening applications. The 2D tumor model is typically represented by a monolayer culture of cells; 3D tumor models (*e.g.*, spheroids, cancer cells encapsulated within scaffolds/hydrogels, microcarriers, and others) can reproduce native cell-cell communication and cell-ECM interactions. Microfluidic chip models can mimic the *in vivo* physiopathology of breast cancer, such as vasculature growth, gradient generation, interstitial flow, or shear stress. Reproduced from [42]. 11
Figure 3: The tumor microenvironment (TME) and the cascade of breast cancer metastasis. Tumor dissemination is initiated by the uncontrolled growth of the tumor and the formation of angiogenesis, a process where new blood vessels are formed from the preexisting ones. These vessels are employed to provide nutrients and oxygen to the tumor. Next, metastatic cancer cells invade the surrounding TME and migrate directionally towards the microvasculature to invade it. Then, these tumor cells travel through the blood vessels as circulating tumor cells to invade distant organs. (e.g., lung, bone, liver, or brain). At the invading stage, cancer cells start proliferating forming a secondary tumor site. Within this project, tumour spheroids were prepared from dissociated cells from circulating tumour cells and ancer cells can be seeded in fabricated scaffolds and in a microfluidic chip platform to model a multiple tissue-type microenvironments. 13
Figure 4: a) A cutaway rendering of the microfluidic array chip shows the six microfluidic channels containing 15 organoids, and the reservoirs. The platform comprises the microfluidic channel structure, a cover layers consisting of twelve connecting holes which are fluidically coupled to the reservoir layer ensuring continuous media perfusion. **b)** Graphical illustration of the microfluidic microarray including hemispherical microwells of diameters of 1000 µm for organoid cultivation on the bottom, microfluidic connector holes and media reservoirs on the top. 21
Figure 5: a) Schematic overview n of different seeding protocols for delivery of metastatic breast cancer organoids (patient-derived organoids; PDOs) from ascites (abdominal cavity) and bone into the biochip. **b)** Comparison analysis of organoid growth from ascites and bone using the different protocols. **c)** Differences in organoid size between cell culture plate and biochip, n=15 ± SD. 22

Figure 6: a) Young's moduli in kPa of different GrowDex® concentrations. **b)** Overview of selected GrowDex® strengths for the preparation of a healthy - and a tumor matrix with a control for comparison to other gels (Matrigel). **c)** Fluorescence staining of nuclei (Hoechst; blue) and proliferating cells (EdU; red) of organoids grown simultaneously over 4 days in different strengths of GrowDex® (GD) in the biochip. The graph shows EdU positive cells compared to total cell number in percent ± SD. 24
Figure 7: Time-resolved growth analysis of patient-derived organoids from human ascites and bone metastasis on-chip. **a)** Bright-field images of PDOs-derived from ascites and bone on-chip cultivated at three different microenvironment stiffnesses (1.3% GD, 0.8% GD, and 0.5% GD) over a cultivation period of 18 days. **b)** Surface area over time of PDOs-derived from ascites and bone cultivated in 1.3%, 0.8%, and 0.5% GrowDex®. **c)** Impact of GrowDex® concentration (%) on PDO area at day 18 post-seeding. 25
Figure 8: Fluorescent-micrographs of EdU- and Ki67-positive cells (1:200 dilution; red) stained either for 40 minutes or overnight (O/N). Cell nuclei were stained by using Hoechst (1:1000 dilution; blue). MCF-7 spheroids were cultivated for one week in 96-well plates embedded imaged in **a, b)** 1.3% GrowDex® (GD) and **c, d)** 1% GrowDex® (GD-T). 26
Figure 9: Time-resolved growth of GFP- positive cancer-associated fibroblasts (CAFs; green) and patient -derived organoids (PDOs) on-chip after **a)** simultaneous and **b)** sequential loading of GrowDex® and GrowDex-T® 28

LIST OF TABLES

Table 1: Patient-derived organoid (PDO) media composition. 16
Table 2: Cancer-associated fibroblast (CAF) media composition. 16
Table 3: Click-iT® EdU was prepared in deionized water according to the manufacturer's protocol. EdU cocktail for 1000 µL: 18

1 BACKGROUND

1.1 THE INTERPLAY OF THE EXTRACELLULAR MATRIX AND ANTI-CANCER DRUG RESISTANCE

As one of the major topics in the life science sector, the multidisciplinary area of cancer research aims to advance biomedical knowledge and treatment strategies.[1] According to the World Health Organization, cancer is responsible for one in six deaths, which makes it the second most common cause of death globally.[2,3] Supporting these recent epidemiological data, the examination of a more extended period and the analysis of the data collected by the National Cancer Institute over the last 40 years showed that there had been a continuous and almost stable increase in incidence rates of all cancers. At the same time, a general decrease in mortality rates was recorded in the last 20 years, although there was a slight increase in mortality rates. This reduction in mortality rates can be easily associated with the continuous progress in the medical and pharmacological fields that has reduced cancer deaths, thanks to the recent introduction in the therapy of more effective drugs and therapeutic approaches.[4]

To date, chemotherapy is, besides radiotherapy and surgery, the most used clinical anti-cancer treatment approach toward cancer-related diseases since 1940.[5] However, chemotherapeutic agents are often unspecific, rapidly cleared from the blood circulation, and present a low accumulation at the tumor site. Moreover, cancer cells can develop resistance mechanisms to anti-cancer drugs from the beginning of the treatment or after several administrations. Consequently, cancer cells can escape the action of the drug leading to decreased therapeutic effect. The increased resistance of cancer cells also contributes to the fact, that progression-free survival of patients after the second line of chemotherapy is lower than after first-line treatment. These diverse mechanisms can either originate inherently in the tumor tissue itself by therapy or mediated by the tumor's environment.[6,7]

In the past decades, previous studies have mainly focused on the cancer cell itself rather than the interactions between cancer cells and their environment. However, the role of the tumor microenvironment (TME) on tumor growth and drug efficacy has attracted much attention in recent years. The TME includes not only cancer cells but also the physical, chemical, and biological components surrounding cancer cells, such as the extracellular matrix (ECM), interstitial flow, stromal cells, immune cells, vascular networks, and biochemical concentration gradients. Recent studies have shown that the physical and biochemical properties of the TME significantly affect cancer progression, including malignancy, invasion, and metastasis. The

TME is often referred to as a "wound that does not heal," based on the tumors invoking programs closely resembling wound healing response in its recruitment and activation of the stroma to induce desmoplasia, similar to scar tissue.[8] This aberrant and fibrotic stroma influences the physical properties of the TME and is very different from the normal stroma.[3] Matrix proteins themselves can increase tumor fitness and drug resistance through multiple mechanisms. For example, the proteoglycan perlecan, secreted by the tumor-educated cancer-associated fibroblasts (CAFs), can induce resistance to chemotherapy[9] and, similarly, fibronectin can induce therapy resistance, contributing both to endocrine and chemotherapy resistance[10]. Additionally, alterations in the composition of the ECM proteins modify the physical properties of the TME. It is well known that the tumor elastic modulus (stiffness) is several times higher than normal tissue counterparts leading to more aggressive and migratory tumors. Interestingly, there also appears to be a threshold after which the stiffness becomes tumor-suppressive again, suggesting a bell-shaped effect on cancer growth and invasion[11].

Stiffer TME also impacts intracellular signaling triggered by integrins, FAK, and c-Src kinases. Secretion of matrix crosslinking enzymes, like collagen prolyl hydroxylases, lysyl hydroxylases, lysyl oxidases, and weaker ECM linkers, such as hyaluronan and proteoglycan link protein 1 by the tumor cells and the CAFs can significantly increase tissue stiffness.[12] These enzymes fold and align the collagen fibers and crosslink them with elastin molecules, making the ECM mechanically durable and stiff, and increasing cancer progression and metastasis, suggesting that mechano-sensing also drives cancer progression.[13,14] This raises the interesting possibility that preventing tissue stiffening could impede cancer progression and that genetically susceptible individuals predisposed to matrix stiffening might be at greater risk for tumors and could benefit from enhanced screening programs.

1.2 BREAST CANCER PROGRESSION AND BIOMECHANICAL PROPERTIES

As one of the most common cancer types, breast cancer is still one deadliest diseases for women.[15] More than 250 000 new breast cancer cases were diagnosed in the United States in 2017, while breast cancer will be diagnosed in 12% of all women in the United States over their lifetimes.[16,17]

In general, the prognosis and survival rates depend mainly on the type and stage of breast cancer. The molecular subtypes of breast cancer based on histological grade and lymph node metastases are vital prognostic and predictive factors. Consequently, classifying breast cancer into relevant molecular subtypes is an essential aspect of therapeutic decision-making. Classical immunohistochemistry markers such as estrogen receptor (ER), progesterone

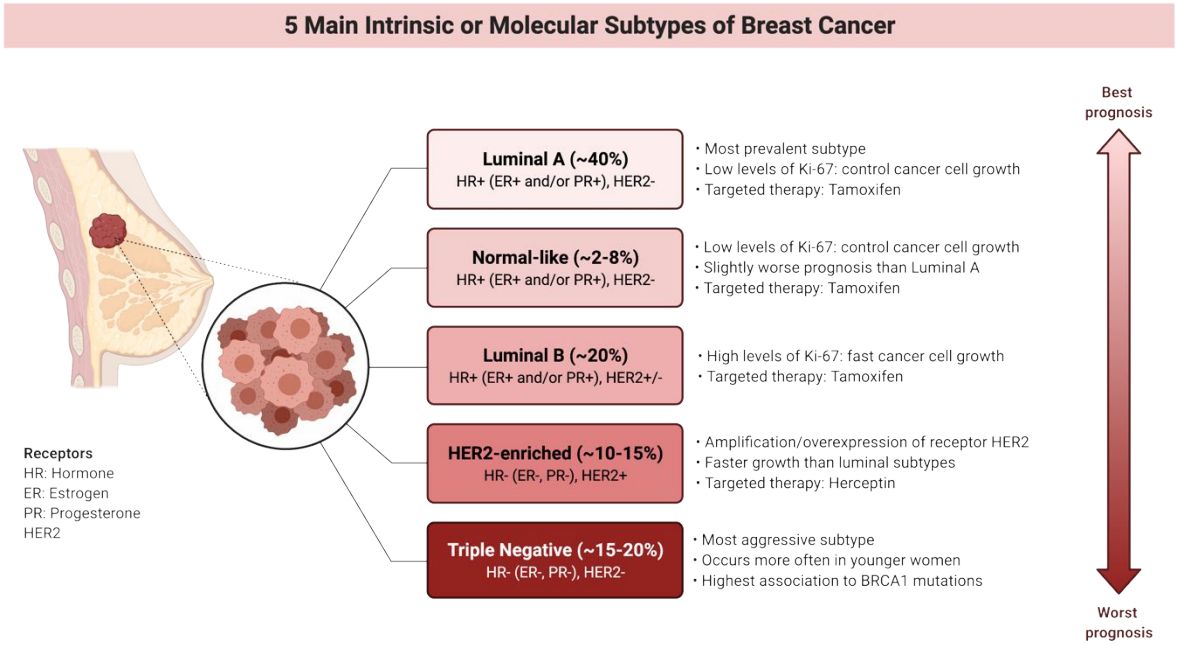

Figure 1: Molecular subtypes of breast cancer. From biorender.com.

receptor (PR), and human epidermal growth factor receptor-2 (HER2) play a crucial role in molecular subtyping.[18] According to the St. Gallen Consensus 2011, molecular subtypes of breast cancer can be classified into Luminal A (ER+/PR+/HER2-/lowKi-67); Luminal B ($ER^+/PR^+/HER2^{-/+}$/high Ki-67); HER2-overexpression ($ER^-/PR^-/HER2^+$), and triple negative breast cancers/TNBCs ($ER^-/PR^-/HER2^-$) as depicted in Figure 1.[19] Thus, it is essential to note that use of techniques enabling molecular subtyping in clinical practice would provide more accurate information about patient-specific prognosis, risk of relapse and probability for a pathological complete response.

In this context, the mechanical properties of breast tissue play a prominent role in the research related to several clinical, pre-clinical, as well as current applications such as self-diagnosis through palpation. These applications include cancer detection, mechanics of injury, surgical simulators, and tumor motion tracking during surgeries. Especially breast cancer is characterized by changes in cellular rheology and tissue level forces, a stiffening of the tissue, and a progressive loss of tensional homeostasis that has been exploited to detect tumors. The mechanical properties of a tissue contribute to disease progression, compromise treatment, and might also alter cancer risk. However, the remodeling that induces these changes can occur for several reasons: For mammary cancers, tumors “feel” stiffer during manual palpation in part from increased ECM expression and cross-linking as well as changes in protein composition.

This dynamic tumor microenvironment is established by tumor and stromal cells and their soluble factors, which evolve as the tumor progresses over months to years.

To study the influences of the TME on breast cancer progression and metastasis, animal models are widely used to recapitulate the dynamics of human tumors, e.g., stiffening by lysyl oxidase-mediated cross-linking.[20] Cancer cell lines and mouse models have therefore provided invaluable insights to the field of breast oncological research, having contributed to the current understanding of the genetic and mechanistic basis of breast cancer development, as well as drug discovery and testing. While these methods will remain important for efficient large-scale screens, two-dimensional (2D) mono-cultures are physiologically dissimilar to patient-specific human tumors, and, in the case of animal models, different immune interactions and inherent heterogeneity denotes the lack of precise control over these systems. For instance, a recent study involving data analysis on a set of 3,290 approved cancer drugs reported 1,637,449 adverse events in regulatory submissions for more than 70 years, indicating an insufficient translation of animal studies to predict human response. [21,22]
To overcome these limitations, there has been a significant push toward the development of three-dimensional (3D) models that accurately reflect the *in vivo* situation. Tools such as microfluidics, 3D printing, and organoids are now commonly employed to develop more physiologic human tumor models. [23]

1.3 THREE-DIMENSIONAL (3D) CELL MODELS FOR CANCER RESEARCH

The immense heterogeneity of human cancers has hampered the development of cancer therapies and contributes to the limited success of drug treatment. Model systems that recapitulate the reality of variable treatment responses need to be utilized for more precise drug development and testing.[24] In fact, the next large strides in cancer treatment success may depend on precision approaches that consider the diverse nature of individual tumors when choosing treatments.[25,26]

To model solid tumors from cancer patients more accurately, research groups have developed and exploited patient-derived xenografts (PDX), whereby fragments of human tumors are implanted directly into immune-deficient mice and grown in a serially transplantable manner. While imperfect, PDX models are currently the most robust way to model diverse human tumors in the laboratory *in vivo*.[25]

Short-term 2D cultures of human breast cancer cells derived from PDX models have been shown to have responses to therapies that recapitulate tumor responses *in vivo*; however, two-dimensional culture methods are unable to replicate the interactions between cells and their extracellular environment because of the complex microenvironment of natural tumors.[27] These interactions are responsible for cell differentiation, proliferation, viability, gene and protein expression, drug metabolism, and other cellular functions.

Therefore, multicellular 3D tumor spheroids or organoids are considered superior models for preclinical evaluation of tumors in cancer therapy due to their more accurate and advanced biology.[28] The three-dimensional organization of cells within the spheroid structure allows direct contact with the extracellular matrix, enabling them to utilize alternative signaling mechanisms for cell growth and survival not readily observed in 2D cell cultures. Similar to human cancers, 3D spheroids exhibit different cell growth rates throughout the cell constructs, and physiologically relevant gradients such as oxygen, nutrients, and waste products are observed. Therefore, 3D cell culture models are widely used in epithelial cancer research to study mechanisms involved in tumor initiation and progression.[29,30]

Especially, patient-derived organoids (PDOs) show strong biological concordance with the tumors from which they are derived. Organoids are 3D cultured multicellular clusters derived from pluripotent stem cells or isolated organ progenitors that differentiate to form an organ-like tissue exhibiting multiple cell types. Organoids have self-renewal and self-organization capabilities and retain the characteristics of the physiological structure and function of their source tumor.[31] As an example, pancreatic and colorectal tumors have been extensively modeled using patient-derived organoids. Gendoo et al. reported good concordance between patient tumors, PDX, and PDO in pancreatic cancer using whole genome analysis.[32] Another study in pancreatic cancer supported this notion and showed that organoids, although primarily clonal, maintain distinct patient phenotypes and respond differently to drug combinations.[33] Patient-derived pancreatic cancer or colorectal cancer organoids are now being used to predict therapeutic responses and facilitate precision medicine for patients. PDOs have also been described for hepatocellular carcinoma, hepatoblastoma, glioblastoma, prostate; bladder, ovarian, breast; gastric, lung; esophageal, kidney, and head and neck cancers.[34,35]

1.4 MICROFLUIDIC TUMOR-ON-A-CHIP MODELS

In order to capture biological systems under physiologically-relevant measurement conditions, microfluidic fabrication techniques have established a basis to produce complex physical environments that specifically mimic organ tissue functions.[36] Microfluidics is associated with the manipulation of small volumes (10^{-9} to 10^{-18} liters) of fluids using microstructures and channels on the order of tens to hundreds of micrometers. Microfluidic systems, or chips, offer several advantages for studying cancer biology due to the physical properties associated with microscale. The combination of 3D cell culture and microfluidics are currently both considered promising models to understand biological systems (see Figure 2).[37]

As an alternative to animal models addressing the complex problem of cancer development and treatment, tumor-on-a-chip technology has emerged as a new tool for cancer studies. Microfabrication, tissue engineering, and materials research have the potential to significantly improve the understanding of cancer biology and enable accelerated and cost-effective drug discovery.[38] To recreate the tumor microenvironment, tumor chip models containing stromal cells such as pericytes, cancer-associated fibroblasts, smooth muscle cells, myofibroblasts, mesenchymal stem cells, and endothelial cells have been developed to form the individual units of the TME *in vitro*.[39] Dendritic cells, T-cells, and macrophages also have been integrated into tumor chips to address the immune response in cancer therapies.[40] So-called "tumor-on-a-chip" systems have previously been used in research for drug testing and metastasis studies and are considered high-throughput personalized medicine approaches using patient-specific cells.[41]

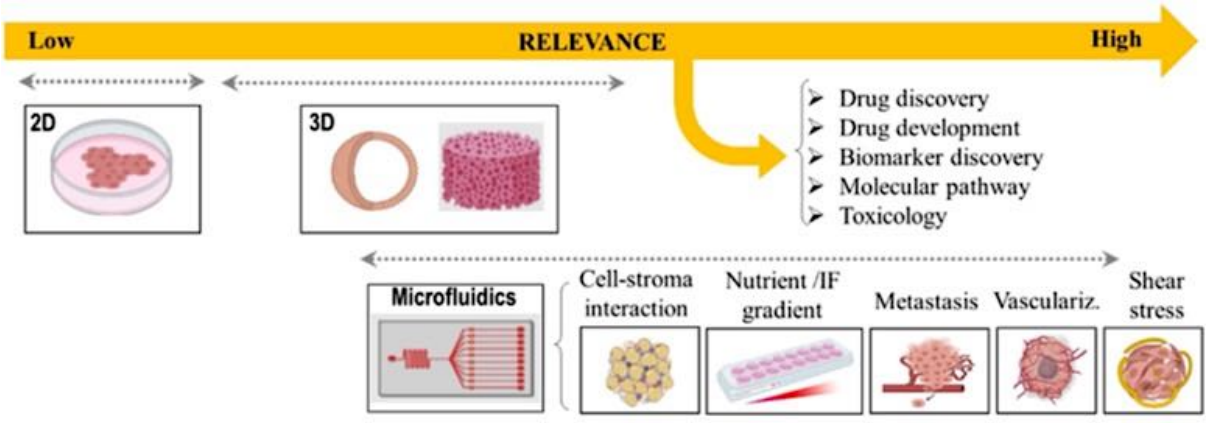

Figure 2: Overview of *in vitro* models for studying breast cancer physiopathology and for drug screening applications. The 2D tumor model is typically represented by a monolayer culture of cells; 3D tumor models (*e.g.*, spheroids, cancer cells encapsulated within scaffolds/hydrogels, microcarriers, and others) can reproduce native cell-cell communication and cell-ECM interactions. Microfluidic chip models can mimic the *in vivo* physiopathology of breast cancer, such as vasculature growth, gradient generation, interstitial flow, or shear stress. Reproduced from [42].

Although the potential of tumor-on-a-chip systems as cancer research tools has been demonstrated through proof-of-concept studies, significant challenges remain in transferring this technology into clinical practice, including the validation and comparison with well-established *in vivo* tumor models. To fully realize the potential of tumor-on-a-chip technology, researchers from the fields of biomedical engineering, materials science, biophysics, cell biology, and oncology must join efforts to develop and optimize novel advanced tumor-on-a-chip systems. [42]

2 AIMS OF THE PROJECT

During the research stay at Harvard Medical School, a novel microfluidic tumor-on-a-chip platform has to be evaluated to monitor the effects of TME stiffness on the proliferation of 3D patient-derived organoids under microfluidic conditions. In this project, specific reactions of 3D organoid cultures from metastatic breast tumor cells (e.g., from bone) will be generated, cultured, and analyzed concerning growth characteristics using an established biochip and compared to state-of-the-art static organoid cultures. Therefore, this research project includes the establishment of physiological tissue structures, including co-culture models of PDOs and CAFs, according to the protocols of Dr. Muranen at Harvard Medical School to evaluate cell proliferation and function in relation to different tumor environments and tissue-specific stiffnesses in the biochip (see Figure 3). The goals, therefore, include (1) the cultivation of tissue-specific structures according to the established protocols of Dr. Muranen on the tumor spheroid chip, (2) the evaluation of tissue architecture and function regarding different tumor milieus to gain insights into their contribution to cell and tissue formation (3) and the drug screening on-chip to gain insight into the promising mechanisms that cells use to develop drug resistance.

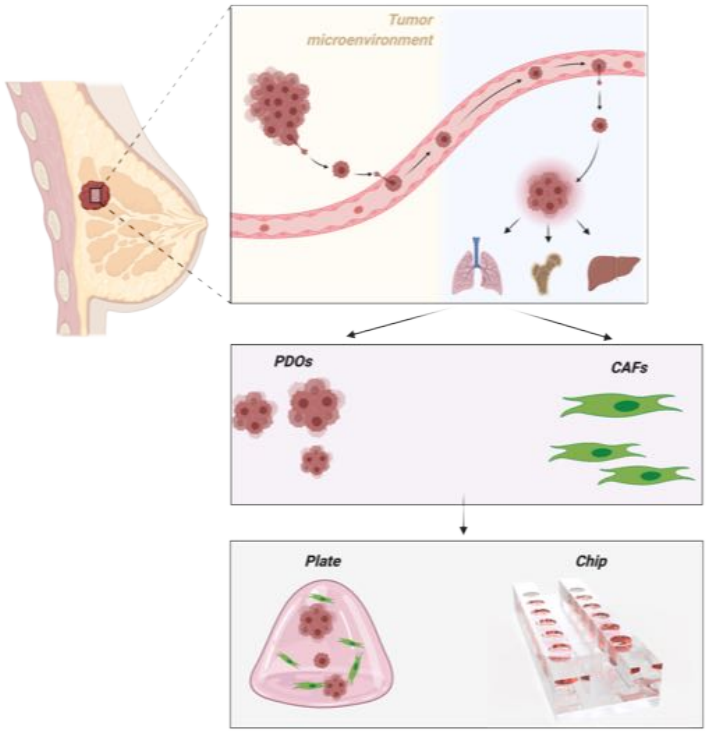

Figure 3: The tumor microenvironment (TME) and the cascade of breast cancer metastasis. Tumor dissemination is initiated by the uncontrolled growth of the tumor and the formation of angiogenesis, a process where new blood vessels are formed from the preexisting ones. These vessels are employed to provide nutrients and oxygen to the tumor. Next, metastatic cancer cells invade the surrounding TME and migrate directionally towards the microvasculature to invade it. Then, these tumor cells travel through the blood vessels as circulating tumor cells to invade distant organs. (e.g., lung, bone, liver, or brain). At the invading stage, cancer cells start proliferating forming a secondary tumor site. Within this project, tumour spheroids were prepared from dissociated cells from circulating tumour cells and ancer cells can be seeded in fabricated scaffolds and in a microfluidic chip platform to model a multiple tissue-type microenvironments.

3 MATERIALS AND METHODS

3.1 MOLD FABRICATION

All applied microfluidic systems were manufactured with Polydimethylsiloxane (PDMS). For the bottom layer of the chip, a soft imprint mold consisting of PDMS was used. The PDMS was thoroughly mixed with the curing agent in a ratio of 1:10 per volume. To remove air bubbles, the mixture was degassed in a desiccator for 45 minutes. The master templates were placed upturned in a petri dish, and then the degassed mixture was poured over the template. The PDMS was cured for two hours at 80°C. Afterward, the master template was peeled off, and the mold was baked for one hour at 120°C. Finally, the mold was silanized. For this step, the mold was plasma treated for two minutes and subsequently coated with trichloro (1H,1H,2H,2H-perfluorooctyl)silane in a desiccator for seven minutes and baked for one hour at 80°C to achieve sufficient evaporation of the silane.

3.2 CHIP FABRICATION

The microwell array system consists of two layers, a bottom and a top layer. The chip was designed to produce 90 size-controlled organoids on one chip with less labor effort as published elsewhere.[43] Each chip consists of six independent cultivation channels. Each channel has a well size of 1000 µm in triplicates, resulting in 15 uniform organoids in each channel. For fabrication, the elastomer curing agent was mixed in a ratio of 1:10 (v/v) with the elastomer base. The mixture was degassed to remove disturbing air bubbles and poured into the two different molds, the lower layer mold and the upper layer mold. The lower layers were cured at 80°C and the upper layers in a 70°C oven for at least two hours. The PDMS surfaces were activated for 30 seconds , 0.6 mbar, and 200W with a plasma oven to crosslink both layers. Subsequently, layers were aligned and baked at 80°C overnight.

3.3 CHIP PREPARATION

To avoid cell attachment, the chips were coated with Lipidure® CM52006. Each channel was filled with 100 µL Lipidure®, and disturbing air bubbles were removed with a short ultrasonic bath treatment. The Lipidure® were evaporated at 80°C for 1 hour, and then chip reservoirs were filled with 70% ethanol. Ethanol was exchanged twice under sterile conditions. To flush the whole channel, all solution exchanges were applied by the aspiration of 200 µL on one reservoir and the addition of 200 µL on the opposite reservoir. After the sterilization, channels

were washed three times with Phosphate-buffered saline (PBS) supplemented with 1% antibiotics. Finally, the channels were flushed twice with cell culture media.

3.4 CELL CULTURE

Patient resection material was cut into small pieces, washed thoroughly, and digested with collagenase. After additional washing and filtration, the digested tissue was plated in basement membrane extract and supplemented with expansion medium (see Table 1). Matrigel® a gel-like substance that polymerizes at temperatures above 37°C, is used to mimic the extracellular matrix and support 3D organoids. Organoid derivation is optimal for tissues that contain a minimal amount of fat and necrotic tissue. The desired epithelial tissue for organoid generation usually appears as firm, pink-to-brownish tissue, whereas necrotic tissue is usually softer and darker. Fat tissue is soft and white to yellow and can be easily scraped or cut off. The split ratio, passage interval, and method of organoid dissociation differ considerably among donors and should be optimized for each newly established organoid culture. Organoids were passaged 7–21 days after organoid establishment.

All cells were maintained at 37 °C in a humidified incubator with 5% CO_2 and were tested negative for mycoplasma contamination. The breast cancer cell line MCF-7 was cultured in Dulbecco's Modified Eagle's Medium (DMEM) with 4.5 g/l glucose and was supplemented with 10% inactivated calf serum, two mM L-glutamine, and 1:100 penicillin-streptomycin. MCF-7pheroids were cultured and generated at 37 °C in ultra-low attachment plates at 37 °C in a humidified environment with 5% CO_2 embedded in various concentrations of GrowDex® or Growdex-T®.

For the generation of CAF primary cultures, tumor-bearing (CAF) tissue pieces were resected from specimens after surgery. Sufficient tumor cell content was verified through analyses of H&E-stained frozen sections. Thereafter, the tissue was cut into small pieces (2–3 mm^3), which were then placed in cell culture flasks and covered with CAF medium (See Table 2) in a humidified environment with 5% CO_2 at 37 °C. When the fibroblasts began to grow from the tissue pieces, the latter were removed, and these cells were cultivated as conventional monolayer cultures. All methods involving human participants were performed following the ethical standards of the institutional committee and with the 1964 Helsinki declaration and its later amendments.

Table 1: Patient-derived organoid (PDO) media composition.

Compound	Concentration
Advanced DMEM/F12 (50 ml)	
Glutamine	2 mM
Glucose	5 mM
HEPES	10 mM
Pen/Strep	1%
Conditioned medium	10%
Heregulin	5 nM
FGF 7	5 ng/ml
FGF 10	20 ng/ml
EGF	5 ng/ml
Noggin	80 ng/ml
A82-01	500 nM
SB202190	500 nM
B27	1X
N-Acetylcysteine	500 µM
Nicotinamide	1 mM
Hydrocortisone	100 ng/ml
Estradiol	1 ng/ml
Nicotinamide	1%

Table 2: Cancer-associated fibroblast (CAF) media composition.

Compound	Concentration
Advanced DMEM/F12 (50 ml)	
FBS	8%
Low Serum Growth Supplement (LSGS)	1X
Pen/Strep	1%

3.5 PATIENT-DERIVED ORGANOID LOADING

Chips were maintained and incubated in quadriPERM filled with 1X PBS supplemented with 1% antibiotic/antimycotic solution to avoid liquid evaporation. In the case of the sequential seeding protocol, 25 µL of PDO suspended media was added to each chip channel. The quadriPERMs containing the chip devices were placed on the rocker platform, set to a flow rate of 13.2 µL/min, and incubated under cell culture conditions (37°C, 5% CO_2). After one hour, channels were filled with respective hydrogel (Matrigel® or GrowDex®), and 100 µL of fresh cell culture media was added to each reservoir. Growth media in devices was changed every two days. In the case of the simultaneous seeding protocol, 25 µL of a mixture of PDOs

and respective hydrogel at different concentrations were introduced to each chip channel. Subsequently, 100 µL cell culture media was added to each reservoir, and media was changed every two days.

3.6 GREEN-FLUORESCENT PROTEIN TRANSFECTION

Transfection can be used in gene therapy to produce recombinant proteins for therapeutic purposes and is essential for lentivirus production.[44] For this method, *E. coli* bacterial strain *STBL3* was used. This strain was designed especially for cloning the direct repeats found in lentiviral expression vectors, and it gives a higher yield of extracted DNA. Lentiviral technology is based on the co-transfection of human cell line HEK293T with packaging, envelope, and transfer plasmids (containing the gene of interest). This has resulted in the assembly of the lentivirus, which, upon transduction, became a powerful tool for expressing exogenous genes into various types of cells both *in vitro* and *in vivo*. A single colony was inoculated with the desired plasmid from the plate with LB (+ antibiotic for selection) into 50 mL of a liquid broth medium with the appropriate antibiotic added. *E. coli* cells were grown at vigorous shaking overnight at 37 °C. DNA purification and quantification was performed according the manufacturer's protocol (PureLink™ HiPure Plasmid Filter Midiprep Kit, cat.no.: K210014, Thermo-Fisher, USA).

Cells were transferred to centrifuge tubes and centrifuged at 4000× *g* for 10 minutes at room temperature. The supernatant was drained, and cells were resuspended in 0.4 mL of resuspension buffer. Then 0.4 mL of lysis buffer was added and mixed gently by inverting the capped tube until the lysate mixture was thoroughly homogenous and incubated for five minutes at room temperature. Next, 0.4 mL precipitation buffer was added and immediately mixed by inverting the tube until the mixture was thoroughly homogeneous, followed by centrifuging the lysate at 12,000 × *g* for 10 minutes at room temperature. The supernatant was loaded onto the equilibrated column and centrifuged at 15,000 × *g* for 10 minutes. The column was washed twice with 2.5 mL wash buffer, centrifuged after each wash, and flow-through was discarded. Then sterile microcentrifuge tube was placed under the column, and 0.9 mL elution buffer was added to the column to elute the DNA and centrifuged at 15,000 × *g* for 10 minutes. 0.63 mL isopropanol was added to the elution tube and centrifuged at 15,000 × *g* for 30 minutes at 4°C. Then, the supernatant was carefully removed and discarded. The DNA pellet was resuspended in one mL 70% ethanol and centrifuged at 15,000 × *g* for 5 minutes at 4°C, followed by the removement of the supernatant. The pellet was air-dried for 30 minutes and resuspended in 50 µL TE buffer. The purity of the plasmids and the concentration were

evaluated using the spectrophotometer NanoDrop (ND-1000). This is a quick method for estimating the amount of extracted DNA and the relative amount of RNA and protein in a sample.

The ratio of absorbance at 260 nm and 280 nm (260/230) is used to measure nucleic acid purity. A good-quality DNA sample should have an absorbance 260/280 ratio of 1.8–2.0. The average absorbance at 260/280 nm for the samples obtained by this method was 1.92. A cell density of 4×10^6 CAF cells was seeded into a 100 mm culture plate one day before the planned transfection with lentiviral vector plasmids. On the day of transfection, cells covered about 80% of the plate surface. On the day after transfection, the medium was changed to fresh DMEM supplemented with 10% FBS, 1% L-glutamine, 1% penicillin/streptomycin, and green-florescent protein (GFP) expression was continuously monitored using fluorescence microscopy.

3.7 PROLIFERATION ASSAY

100 µL of EdU (5-ethynyl-2'-deoxyuridine) reagent (1:1000 in media) were added to cells and incubated for respective periods. PDOs were fixed with 4% paraformaldehyde (PFA) for 40 minutes and washed 3x5 minutes with PBS subsequently. Then, PDOs were permeabilized for 20 minutes with 0.5% TritonX-100 (TX-100) in PBS at room temperature (RT) and washed 2x5 minutes with PBS. Cells were incubated for 40 minutes with EdU cocktail mix:

Table 3: Click-iT® EdU was prepared in deionized water according to the manufacturer's protocol. EdU cocktail for 1000 µL:

Compound	**Volume (µL)**
EdU reaction buffer (1X)	860
CuSO4	40
Alexa Fluor 459	2.5
Reaction buffer additive (1x)	100

Samples were then blocked for one hour with 0.3% TX-100, 0.5% BSA, and 5% goat serum. Primary antibody (Rabbit anti-ER) was diluted 1:100 and incubated overnight at 4°C. Samples were washed ten times with 0.3% TX-100 in PBS. Secondary antibody (Alexa Fluor 488) was diluted 1:500 and applied for two hours at RT. after incubation, samples were again washed 1o times with 0.3% TX-100 in PBS. Cell nuclei were counterstained with Hoechst (1:1000 in PBS) and for 15 minutes and washed with PBS before mounting with Vectashield.

3.8 IMMUNOHISTOCHEMISTRY

To visualize PDO-specific marker expression and proliferation, immunohistochemistry was performed. Medium from each well was aspirated and immediately fixed with 4% PFA for 20 minutes at room temperature. Cells were permeabilized with PBS containing 0.5% Triton X-100 for 10 minutes at 4°C. Samples were then rinsed three times with PBS/Glycine (130 mM NaCl; 7 mM Na_2HPO_4; 3.5 mM NaH_2PO_4; 100 mM glycine), 15 minutes per wash at room temperature. Samples were blocked with 200 µL/well of IF Buffer (130 mM NaCl; 7 mM Na_2HPO_4; 3.5 mM NaH_2PO_4; 7.7 mM NaN_3; 0.1% BSA; 0.2% Triton X-100; 0.05% Tween-20) +10% goat serum overnight at 4°C. Primary antibody was incubated in block solution at a 1:200 dilution overnight at 4°C. Samples were rinsed three times (20 minutes each) with PBS at room temperature with gentle rocking.

Then conjugated secondary antibody in IF Buffer + 10% goat serum was applied for overnight min at room temperature at 1:200 dilution. Samples were rinsed once for 20 minutes with IF Buffer at 4°C, followed by gentle rinsing 3 times with PBS (20 minutes). In order to counterstain nuclei, cells were incubated with PBS containing for 15 minutes at room temperature.

3.9 IMAGE ACQUISITION

For confocal imaging, the cells were grown on No. 1.5. All confocal images were collected with a Zeiss LSM 880 confocal microscope. DAPI fluorescence was excited with the 404 nm laser line with a solid-state laser and a 450/50 emission filter. Alexa-488 was excited with 488 nm Argon-krypton laser with a 525/50 emission filter. Alexa-568 was excited with 561 nm solid-state laser with a 595/50 emission filter, and the Alexa-647 was excited with a 640 nm solid-state laser with a 700/75 emission filter. Images were acquired with the Nikon Elements acquisition software. For figures on EDU and Ki67 positive cells, confocal z-series were taken, five optical sections were collected with a step size of 0.125 microns, using a TiZdrive. Z-series are shown as maximum z-projections and were processed by the Nikon Elements software. Light microscopy was used to obtain images of cells in culture.

3.10 IMAGE ANALYSIS

Image analysis was performed with the ImageJ 1.52 Fiji analysis software and Zeiss Zen Black imaging software. For fluorescence intensity comparisons, images were acquired at identical settings, and intensity was analyzed. Proliferation images were quantitated from maximum

intensity projections confocal z-sections of cells, and number of Hoechst-positive and EdU/Ki67-positive cells were analyzed separately, and ratio was calculated. For other intensity quantifications, the background was measured and, if found similar in all conditions, was not subtracted.

3.11 STATISTICAL ANALYSIS

All experiments were repeated at least three independent times. Data represent the mean ±SD unless otherwise indicated. In comparing two groups, a two-tailed non-paired Student's t-test was conducted. One-Way ANOVA determined statistical analysis with Kruskal-Wallis One Way Analysis of Variance on Rank, or Two-Way ANOVA with all pairwise multiple comparison Holm-Sidak using Graphpad Prism 8.

4 RESULTS

4.1 MICROFLUIDIC MICROARRAY CONCEPT FOR THE GENERATION, CULTURE, AND ANALYSIS OF PATIENT-DERIVED BREAST CANCER ORGANOIDS

The microfluidic device enables the culturing of 3D organoids with high reproducibility in medium- to high-throughput formats. The microfluidic multi-organoid microarray thus closes an essential technological gap, enabling rapid and easy production of organoids of defined sizes and cell types. This device can be operated without the need for a pump and relies on gravity-driven perfusion. The flow speed is modulated by adjusting the tilting angle and speed of a conventional laboratory rocker. Scaling is achieved by generating 90 PDOs on one chip and 360 PDOs on a microtiter plate format. Media reservoirs are arranged at a pitch of 9 mm and were therefore conveniently addressable with standard multichannel pipettes for 96-well microtiter plates.

In detail, the chip shown in Figure 1a is comprised of three main components: (1) microfluidic culture channels in a standard 96-well plate footprint with microwells, (2) perfusion connectors incorporated into the cover layer of the channel structures that interconnect the inlets and outlets of culture channels with media reservoirs, and (3) a pair of media reservoirs for each culture channel, which facilitates a straightforward and easy-handling cell seeding method and

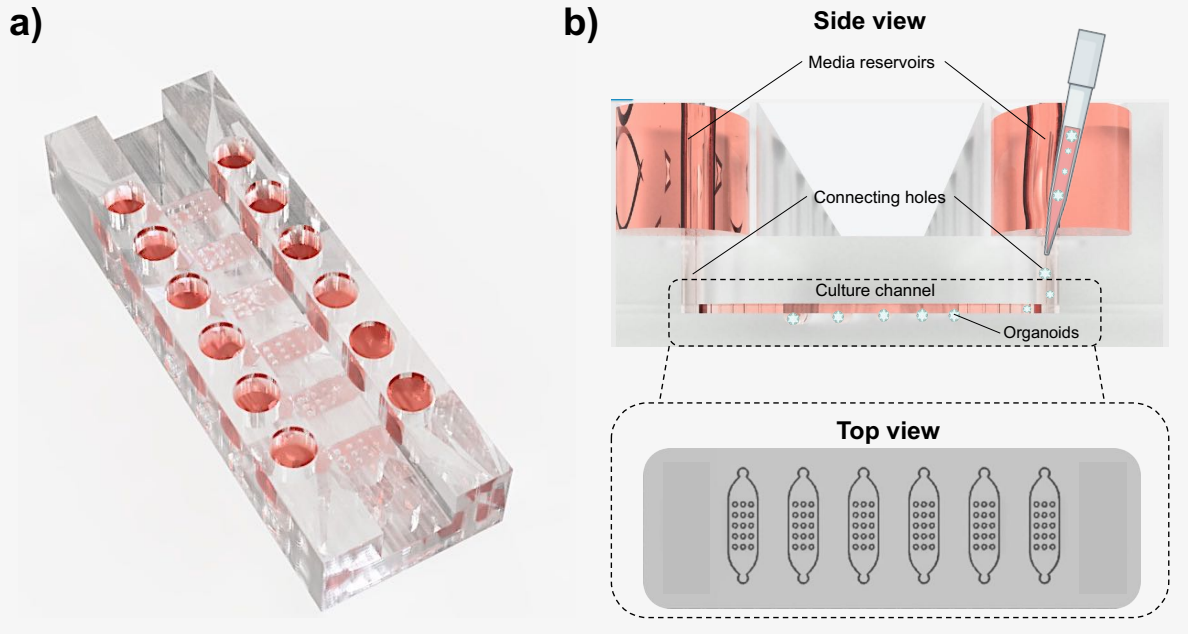

Figure 4: a) A cutaway rendering of the microfluidic array chip shows the six microfluidic channels containing 15 organoids, and the reservoirs. The platform comprises the microfluidic channel structure, a cover layers consisting of twelve connecting holes which are fluidically coupled to the reservoir layer ensuring continuous media perfusion. **b)** Graphical illustration of the microfluidic microarray including hemispherical microwells of diameters of 1000 µm for organoid cultivation on the bottom, microfluidic connector holes and media reservoirs on the top.

retrieval of media or cellular material. A rendered cutaway of the platform (see Figure 1b) shows the microfluidic channels of the microfluidic biochip constructed by soft-lithography from PDMS. The chip enables a parallel loading of 6 channels, where cells form organoids due to surface modification with a biocompatible low-adhesive 2-(methacryloyoxy)ethyl phosphorylcholine (MPC) polymer. After organoids are formed, cells and tissues can be imaged with high-resolution microscopy from the bottom. The system enables parallel screening of different TMEs and treatment scenarios and the generation of highly robust and complete data sets, including measuring dynamic tissue behavior with temporal resolution.

4.2 Optimization of the patient-derived organoid seeding protocol

To evaluate stable cultivation conditions of breast cancer organoids in the biochip, different protocols for introducing the cell material were established and tested based on literature research (see Figure 1a). Here, metastatic breast tumor organoids were isolated from the abdominal cavity (ascites) and bone, subsequently introduced into the microfluidic biochip, and incubated for four days. As shown in Figure 1b, the simultaneous seeding protocol involving embedded PDOs in Matrigel® resulted in unreliable organoid trapping in microcavities indicated by a random distribution of cell clusters of both tissue types in the cultivation channels (see white arrows in Figure 1b).

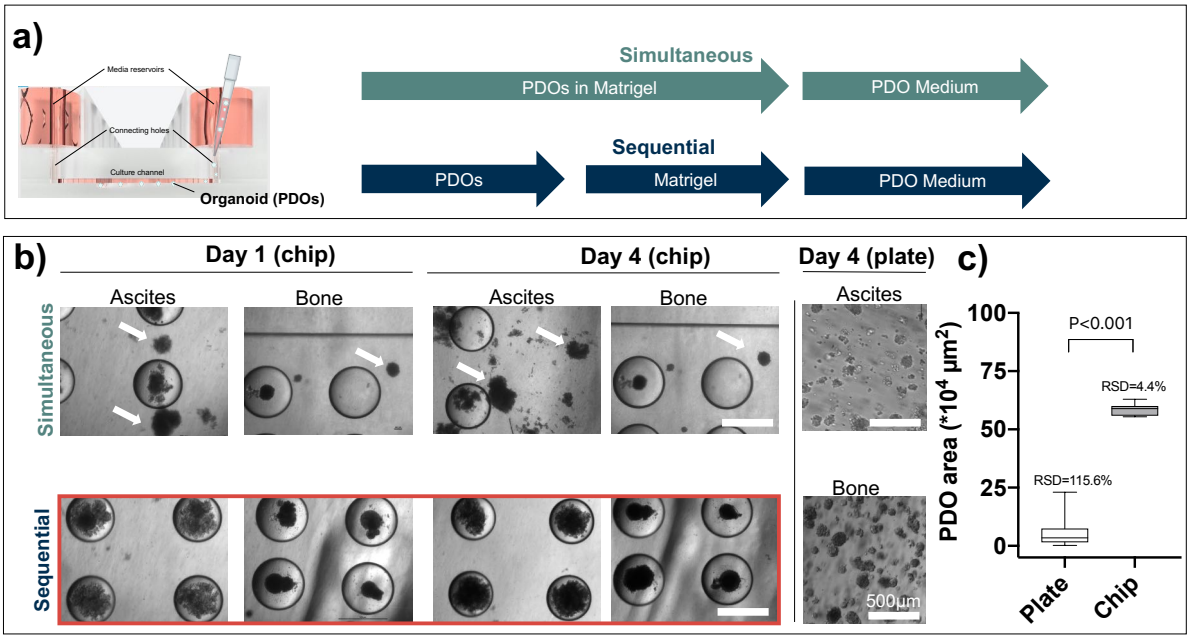

Figure 5: a) Schematic overview n of different seeding protocols for delivery of metastatic breast cancer organoids (patient-derived organoids; PDOs) from ascites (abdominal cavity) and bone into the biochip. **b)** Comparison analysis of organoid growth from ascites and bone using the different protocols. **c)** Differences in organoid size between cell culture plate and biochip, n=15 ± SD.

In contrast, sequential integration of organoids was revealed to be the more effective cultivation method, as stable localization of both tumor organoid types in individual microwells was achieved. A comparative analysis of the PDO area showed that organoid chip cultures exhibited an 11-fold higher surface area than tissue culture plates. Additionally, more reproducible tumor sizes could be generated relative to the conventional cultivation method, as shown in Figure 1c. In detail, PDOs cultivated on-chip exhibited a mean surface area of $58.5 \pm 2.6 * 10^{-4}$ µm^2 at a relative standard deviation (RSD) of 4%, while organoids on the plate showed a significant reduction of size and reliability indicated by an area of $5.2 \pm 6.9\ 10^{-4}$ µm^2 and an RSD of 116%. This can be concluded to the specific design of the biochip microstructure of the biochip, and the smaller channel volumes and surface result in uniform distribution of the cell material after injection.

4.3 TUMOR MICROENVIRONMENT STIFFNESS MODULATION ON-CHIP

Next, the effects of various tumor microenvironments on organoid proliferation were tested on-chip. In this context, commercially available hydrogel (GrowDex®) was used, which can achieve the specific strengths of the breast tissue as well as the tumor tissue through the individual dilution steps of the gel. In the past, various kinds of polysaccharides molecularly dissolved in aqueous media have been used scaffolds for tissue engineering, but typically they require a separate cross-linking step to form the hydrogel network. Many animal-derived hydrogels as Matrigel® contain growth factors, other biological signaling molecules, and unknown amounts of different ECM proteins and have also suffered from variation between lots. In order to avoid the unknown factors in the culture system, the development of clean 3D culture scaffolds that are xeno-free, stable, and non-inducing is essential for improving the relevancy and repeatability of *in vitro* models.[45] In this project, a nanofibrillar cellulose hydrogel GrowDex® derived from the abundant plant sources provide these desired functionalities such as a) rheological properties that allow the formation of a 3D scaffold, 2) cellular biocompatibility without added growth factors, 3) cellular polarization, and 4) differentiation and proliferation of human primary cells. At high shear stress, the aqueous hydrogel has small viscosity that supports injectability, whereas, at low shear stress conditions, the material is converted to an elastic gel. Due to the inherent biocompatibility without any additives, GrowDex® generates a feasible and sustained microenvironment for 3D cell culture and tissue engineering.[46] The graph in Figure 6a shows that Young's moduli can be tuned easily by adjusting gel concentration over a broad range of stiffnesses up to 5 kPa. Therefore,

a)

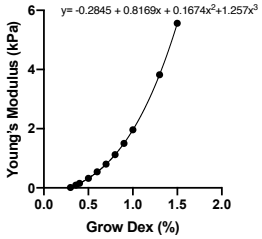

b)

GrowDex® (%)	Stiffness (kPa)	Status
1.3	4.1	Tumor
0.8	1.1	Healthy
0.5	0.4	Control (Matrigel)

c)

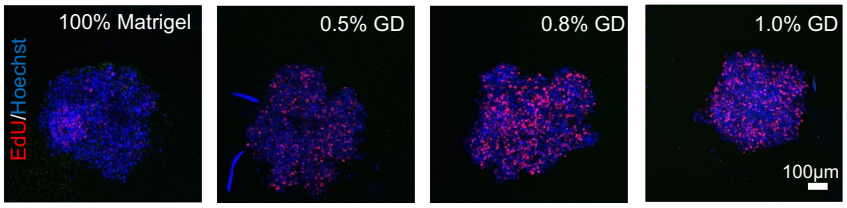

d)

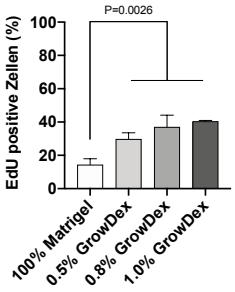

Figure 6: a) Young's moduli in kPa of different GrowDex® concentrations. **b)** Overview of selected GrowDex® strengths for the preparation of a healthy - and a tumor matrix with a control for comparison to other gels (Matrigel). **c)** Fluorescence staining of nuclei (Hoechst; blue) and proliferating cells (EdU; red) of organoids grown simultaneously over 4 days in different strengths of GrowDex® (GD) in the biochip. The graph shows EdU positive cells compared to total cell number in percent ± SD.

GrowDex® has been shown to be a promising matrix for the use with patient-derived organoids cultured within the areas of drug screening tests and personalized medicine.

Since stiffening occurs in breast tissue due to pathological changes in breast cancer, a higher strength (4.1 kPa) was anticipated compared to healthy tissue (1.1 kPa). Matrigel® was used as a control since this hydrogel is widely used to cultivate organoids but does not meet physiological-relevant stiffness levels, as shown in Figure 6b. Figure 6c showed immunochemical sections of the proliferation marker EdU (5-ethynyl-2'-deoxyuridine)-positive cells in red. Since this first experiment aimed to evaluate the impact of stiffness levels on EdU staining performance, GrowDex® concentrations of 0.5%, 0.8%, and 1.0% were used. However, results in Figure 6d exhibited an up to 2.7-fold higher proliferation of GrowDex®-embedded organoids compared to Matrigel®-embedded organoids. Furthermore, a slight trend towards stiffness-dependent proliferation was observed, which, however, could not be statistically proven in these studies.

4.4 TIME-RESOLVED MULTI-TUMOR TISSUE GROWTH MONITORING ON-CHIP

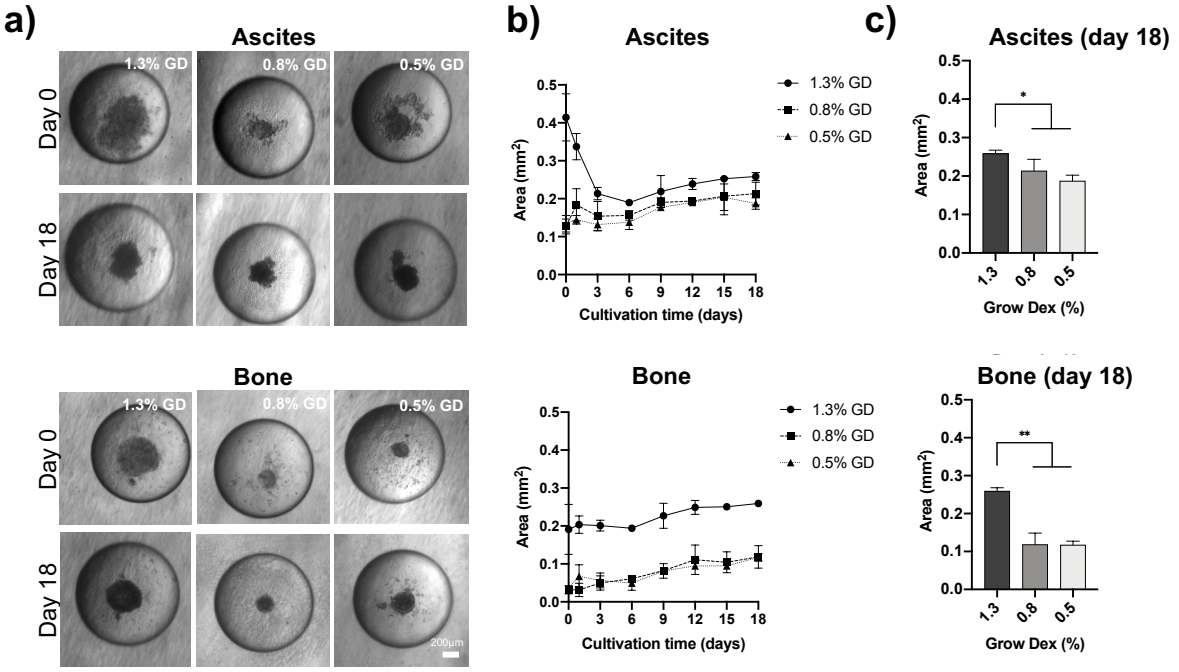

Figure 7: Time-resolved growth analysis of patient-derived organoids from human ascites and bone metastasis on-chip. **a)** Bright-field images of PDOs-derived from ascites and bone on-chip cultivated at three different microenvironment stiffnesses (1.3% GD, 0.8% GD, and 0.5% GD) over a cultivation period of 18 days. **b)** Surface area over time of PDOs-derived from ascites and bone cultivated in 1.3%, 0.8%, and 0.5% GrowDex®. **c)** Impact of GrowDex® concentration (%) on PDO area at day 18 post-seeding.

To evaluate tissue-related PDO growth over time, size-depended differences of tumor organoids from metastasis from ascites and bone were investigated on-chip. PDOs were injected into the microfluidic chip platform by using the validated sequential seeding protocol, as described before, over a cultivation period of 18 days. To assess the influence of TME stiffness on growth, three physiological-relevant GrowDex® compositions (see Figure 6b) of 1.3%, 0.8%, 0.5% were tested in parallel. Bright-field micrographs in Figure 7a showed time-depended size and morphological changes of both ascites, and bone PDOs on the chip. Tumor organoids from the ascites showed a significant decrease of the surface area of 48% in the first three days of cultivation at the highest stiffness of 1.3%, while PDOs at lower stiffnesses (0.8% and 0.5%) exhibited comparable morphology during that time frame. In the next days of cultivation, organoid surfaces increased gradually at all GrowDex® concentrations of 1.3%, 0.8%, and 0.5% by 17.4%, 27.9%, and 33.9%, respectively. In the case of PDOs derived from bone, a stable increase of size could be determined at all Matrix compositions, indicated by surface area growth of 26.2%, 73.2%, 68.4% at concentrations of 1.3%, 0.8%, 0.5% GrowDex® from day 0 to day 18 post-seeding. These results indicated a compressions-effect of high Matrix

stiffnesses (1.3%) on ascites metastasis, while PDOs from bone metastasis remained unaffected by higher Young's moduli, suggesting possible tissue-specific behavior in TME compositions. Surface area analysis in Figure 6c revealed matrix stiffness-related differences in both tumor tissue types at day 18 post-seeding. Significant higher surface areas up to 155% could be achieved at GrowDex® stiffness of 1.3% for both tumor types, while lower concentrations of 0.8% and 0.5% resulted in comparable sizes.

4.5 Optimization of Proliferation Marker Staining Protocols

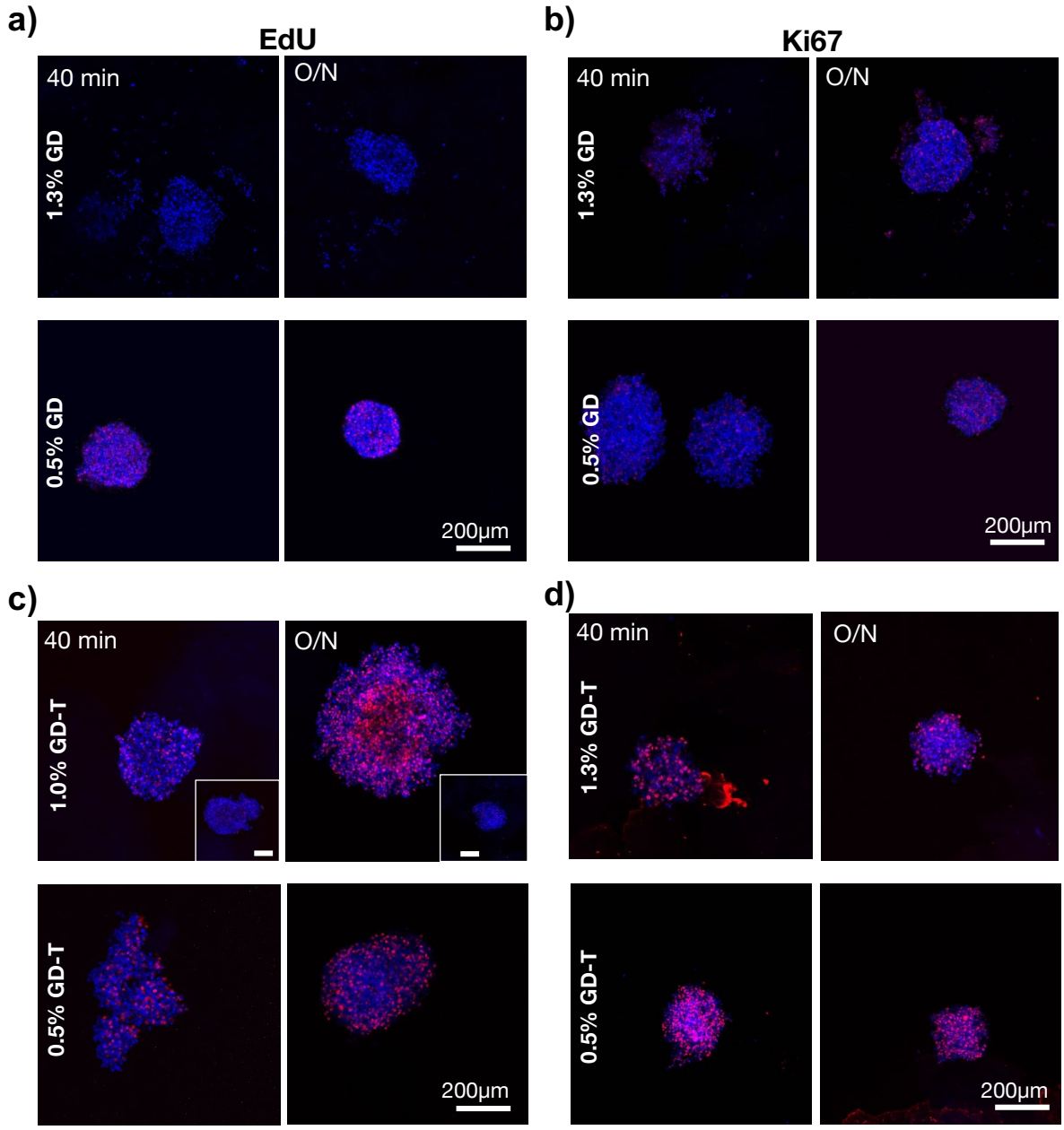

Figure 8: Fluorescent-micrographs of EdU- and Ki67-positive cells (1:200 dilution; red) stained either for 40 minutes or overnight (O/N). Cell nuclei were stained by using Hoechst (1:1000 dilution; blue). MCF-7 spheroids were cultivated for one week in 96-well plates embedded imaged in **a, b)** 1.3% GrowDex® (GD) and **c, d)** 1% GrowDex® (GD-T).

Since matrix-dependent alterations in proliferation marker signals resulted in non-reproducible data outcomes in previous experiments (data not shown), EdU and Ki67 staining protocols were further optimized and evaluated. To investigate the effects of matrix stiffnesses and GrowDex® types on imaging modalities, two well-known proliferation markers, EdU and Ki67, were applied to embedded MCF-7 spheroids for 40 minutes and overnight. According to the manufacturer, GrowDex®-T is ready to use hydrogel that has been specifically developed to offer superior imaging properties compared to the original hydrogel GrowDex® (GD). Results in Figure 8ab showed EdU- and Ki67-positive cells in MCF-7 spheroids embedded in 1.3% and 0.5% GD after 40 minutes as well as after overnight incubation. In the case of GrowDex-T® (GD-T), Ki67-positive cells could be identified even after 40 minutes of primary antibody incubation, in contrast to reduced EdU fluorescence signal in embedded MCF-7 spheroids as shown in Figure 8cd. Results, therefore, exhibited higher staining and imaging performance using GrowDex-T® embedded MCF-7 spheroids and Ki67 as a more reliable marker compared to GrowDex® and EdU.

4.6 ESTABLISHMENT OF BREAST CANCER CO-CULTURE MODEL ON-CHIP

To further increase the biological relevance, a co-culture protocol for the additional introduction of cancer-associated fibroblasts (CAFs) into the microfluidic chip platform was established. To monitor the time course of CAFs growth in the presence of organoids, the fibroblasts were GFP-labeled by transfection of a plasmid, which was produced biotechnologically beforehand (see Materials and Methods section).

In this regard, again, sequential and simultaneous seeding protocols including PDOs and CAFs were evaluated. This experiment involves a simultaneous introduction of PDOs and CAFs followed by 1% GrowDex® or 1% GrowDex-T® after 1 hour into the biochip, as depicted in Figure 9a. A reduced concentration of 1% was chosen to avoid extensive use of expensive hydrogel and since CAFs are known to react very sensitive to synthetic matrices.

In the case of the sequential approach, PDOs and CAFs were first seeded as a co-culture into the biochip, and the two GrowDex® types were added after one day of cultivation (see Figure 9b). The results showed a successful seeding of PDOs and CAFs in both protocols, indicated by a precise location and positioning of the cells in each microwell of the chip at day 0. Different effects of the GrowDex® types (GrowDex® and GrowDex-T®) could be observed at day 1, shown by a CAF fluorescent signal loss in the GrowDex-T® scenario, stemming from lack of cell proliferation. A similar effect was detected for the simultaneous protocol after one day of GrowDex-T® cultivation (data not shown). It is suggested that the limited nutrient supply

in the GrowDex-T® resulted in cell death since the stock solution of GrowDex-T® (1%) do not require any dilution steps with cell culture media to reach a final concentration of 1%, while standard GrowDex® has to be diluted from 1.3% to 1% to achieve the same concentration. Therefore, the simultaneous protocol using 1% GrowDex contained sufficient nutrients for cultivation, exhibited the best seeding performance, and should be considered as the principal approach for establishing a breast cancer co-culture model in the microfluidic array.

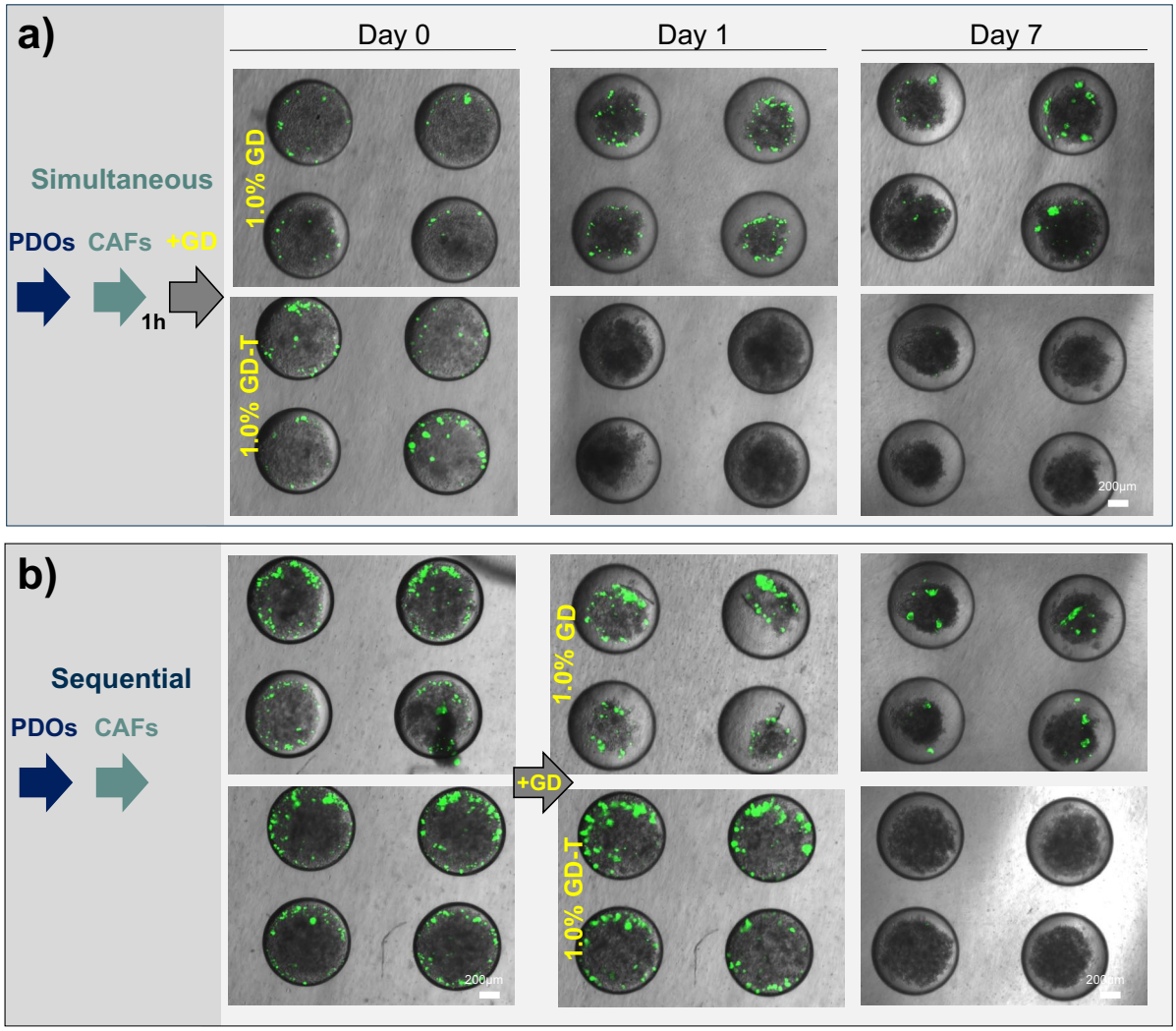

Figure 9: Time-resolved growth of GFP- positive cancer-associated fibroblasts (CAFs; green) and patient -derived organoids (PDOs) on-chip after **a)** simultaneous and **b)** sequential loading of GrowDex® and GrowDex-T®.

5 DISCUSSION

Breast cancer research is an active field of study, complicated by its various subtypes and classifications. Although 2D assays and complex animal models have provided significant insights into cancer development and progression to date, there remains a lack of well-established physiological *in vitro* 3D breast cancer models. Novel microfluidic technologies now importantly incorporate key features of the breast tumor microenvironment, allowing for novel targets to be examined. Integration of patient cells and the development of adaptive high-throughput models are considered to improve breast cancer treatment specificity and allow for *in vitro* tool adoption for personalized medicine. The current models have revealed critical insight into breast cancer biology, yet they are still in their infancy and require further development prior to the implementation as preclinical tools. [47]

Current 3D culture methodologies are diverse, resulting in tumor organoids that vary in size, morphology, and complexity. This leads to challenges in obtaining standards with respect to culture and assay protocols and output data for any given cell type. Much effort is still needed to ensure reproducibility, high throughput analysis capacity, compatibility of readout techniques, and better automation to establish standardized and validated 3D cell models. Taken together, the need to use more physiologically relevant 3D spheroid and organoid models for *in vitro* testing and the need to develop standardized, automated, scalable 3D systems are driving innovations to improve the quality, consistency, and predictive capacity of these cultures.

In the research stay at the Harvard Medical School, a microfluidic chip system for patient-derived organoid screening was characterized to demonstrate the compatibility, usability, and throughput of a microfluidic platform that was established within the framework of a dissertation at the Technische Universität Wien to produce and analyze complex breast cancer models.

The operation of the chip relies on gravity-driven flow and does not require specialized equipment, such as external tubing or expensive precision pumps. Nevertheless, flow rates could reliably be established and modulated, and a wide range of flow rates could be applied on-demand. The performance of the microfluidic device in combination with the co-culture of PDOs and CAFs demonstrates the flexibility of the system and the wide range of possible applications in life science.

Although the established biochips hold great potential for large-scale integration in industrial applications, however, the chip has to be redesigned for future approaches to enable automated imaging of multiple or sequential biopsies at a single time to provide valuable information about tumor development. In combination with automated optical imaging techniques into breast tumor on-chip systems together with data interpretation tools it is expected to provide physicians and pharmaceutical industries with new hope for understanding the cancer development and to shed light on the possible therapeutic approaches.

Finally, it is worth noting that microfluidics still faces some challenges, which need to be solved before being adopted by the clinics. For the particular case of breast tumor-on-a-chip models, the integration of different cell types and tissues of specific breast metastatic sites with varying requirements of media is still a limitation that needs to be addressed. Further, the limited availability of the primary cells and tissue samples from a breast cancer patient is another hurdle in this field. The use of human iPSCs holds very promisingly for the generation of relevant on-chip models. Next, the broad use and implementation of xeno-free biomaterials would help to recreate better the biochemical and structural complexity of the native 3D microenvironment. Since tumor-specific matrix stiffness above 1.0% of GrowDex® resulted in significant issues with imaging, biomarker selection, and co-cultures using CAFs, other matrices as GelMa or polyacrylamide should be considered for future studies, knowing that matrix composition at higher Young's moduli remain a concern in the field of organoid culturing. It is challenging to conduct multiple processes, such as biomarker separation, detection, analysis, and retrieval of information from a single chip, from a technological perspective. In addition, further refinement to current models may include the generation of precise gradient flows and shear stresses as relevant mechanochemical cues required for endothelial cells and breast cancer cells, reproducing the *in vivo* conditions.

Overall, despite the current technological and biological limitations, the established breast tumor-on-chip model within this project holds great potential due to its ease of use, efficiency, and relevance for parallel screening of breast tumor proliferation from patient samples.

6 REFERENCES

1 The global challenge of cancer. *Nature cancer* **1**, 1-2, doi:https://doi.org/10.1038/s43018-019-0023-9 (2020).

2 Siegel, R. L., Miller, K. D. & Jemal, A. Cancer statistics, 2018. *CA Cancer J Clin* **68**, 7-30, doi:10.3322/caac.21442 (2018).

3 Roma-Rodrigues, C., Mendes, R., Baptista, P. V. & Fernandes, A. R. Targeting Tumor Microenvironment for Cancer Therapy. *Int J Mol Sci* **20**, doi:10.3390/ijms20040840 (2019).

4 Miller, K. D. *et al.* Cancer treatment and survivorship statistics, 2016. *CA Cancer J Clin* **66**, 271-289, doi:10.3322/caac.21349 (2016).

5 Chabner, B. A. & Roberts, T. G., Jr. in *Nat Rev Cancer* Vol. 5 65-72 (2005).

6 Housman, G. *et al.* Drug resistance in cancer: an overview. *Cancers (Basel)* **6**, 1769-1792, doi:10.3390/cancers6031769

10.3390/cancers6031769. (2014).

7 Park, I. H., Lee, K. S. & Ro, J. Effects of second and subsequent lines of chemotherapy for metastatic breast cancer. *Clin Breast Cancer* **15**, e55-62, doi:10.1016/j.clbc.2014.09.001

10.1016/j.clbc.2014.09.001. Epub 2014 Oct 16. (2015).

8 Kozlova, N., Grossman, J. E., Iwanicki, M. P. & Muranen, T. The Interplay of the Extracellular Matrix and Stromal Cells as a Drug Target in Stroma-Rich Cancers. *Trends Pharmacol Sci* **41**, 183-198, doi:10.1016/j.tips.2020.01.001 (2020).

9 Vennin, C. *et al.* CAF hierarchy driven by pancreatic cancer cell p53-status creates a pro-metastatic and chemoresistant environment via perlecan. *Nat Commun* **10**, 3637, doi:10.1038/s41467-019-10968-6 (2019).

10 Sampayo, R. G. *et al.* Fibronectin rescues estrogen receptor α from lysosomal degradation in breast cancer cells. *J Cell Biol* **217**, 2777-2798, doi:10.1083/jcb.201703037 (2018).

11 Li, Y., Fanous, M. J., Kilian, K. A. & Popescu, G. Quantitative phase imaging reveals matrix stiffness-dependent growth and migration of cancer cells. *Sci Rep* **9**, 248, doi:10.1038/s41598-018-36551-5 (2019).

12 Kaur, A. *et al.* Remodeling of the Collagen Matrix in Aging Skin Promotes Melanoma Metastasis and Affects Immune Cell Motility. *Cancer Discov* **9**, 64-81, doi:10.1158/2159-8290.CD-18-0193 (2019).

13 Oudin, M. J. & Weaver, V. M. Physical and Chemical Gradients in the Tumor Microenvironment Regulate Tumor Cell Invasion, Migration, and Metastasis. *Cold Spring Harb Symp Quant Biol* **81**, 189-205, doi:10.1101/sqb.2016.81.030817 (2016).

14 Trichet, L. *et al.* Evidence of a large-scale mechanosensing mechanism for cellular adaptation to substrate stiffness. *Proc Natl Acad Sci U S A* **109**, 6933-6938, doi:10.1073/pnas.1117810109 (2012).

15 Sung, H. *et al.* Global Cancer Statistics 2020: GLOBOCAN Estimates of Incidence and Mortality Worldwide for 36 Cancers in 185 Countries. *CA Cancer J Clin* **71**, 209-249, doi:10.3322/caac.21660 (2021).

16 DeSantis, C. E. *et al.* Breast cancer statistics, 2019. *CA Cancer J Clin* **69**, 438-451, doi:10.3322/caac.21583 (2019).

17 Waks, A. G. & Winer, E. P. Breast Cancer Treatment: A Review. *JAMA* **321**, 288-300, doi:10.1001/jama.2018.19323 (2019).

18 Viale, G. The current state of breast cancer classification. *Ann Oncol* **23 Suppl 10**, x207-210, doi:10.1093/annonc/mds326 (2012).

19 Goldhirsch, A. *et al.* Strategies for subtypes--dealing with the diversity of breast cancer: highlights of the St. Gallen International Expert Consensus on the Primary Therapy of Early Breast Cancer 2011. *Ann Oncol* **22**, 1736-1747, doi:10.1093/annonc/mdr304 (2011).

20 Ondeck, M. G. *et al.* Dynamically stiffened matrix promotes malignant transformation of mammary epithelial cells via collective mechanical signaling. *Proc Natl Acad Sci U S A* **116**, 3502-3507, doi:10.1073/pnas.1814204116 (2019).

21 Arrowsmith, J. Trial watch: phase III and submission failures: 2007-2010. *Nat Rev Drug Discov* **10**, 87, doi:10.1038/nrd3375 (2011).

22 Waring, M. J. *et al.* An analysis of the attrition of drug candidates from four major pharmaceutical companies. *Nat Rev Drug Discov* **14**, 475-486, doi:10.1038/nrd4609 (2015).

23 Trujillo-de Santiago, G. *et al.* The Tumor-on-Chip: Recent Advances in the Development of Microfluidic Systems to Recapitulate the Physiology of Solid Tumors. *Materials (Basel)* **12**, doi:10.3390/ma12182945 (2019).

24 Woo, X. Y. *et al.* Conservation of copy number profiles during engraftment and passaging of patient-derived cancer xenografts. *Nat Genet* **53**, 86-99, doi:10.1038/s41588-020-00750-6 (2021).

25 Byrne, A. T. *et al.* Interrogating open issues in cancer precision medicine with patient-derived xenografts. *Nat Rev Cancer* **17**, 254-268, doi:10.1038/nrc.2016.140 (2017).

26 Clohessy, J. G. & de Stanchina, E. Infrastructure needs for translational integration of mouse and human trials. *Cold Spring Harb Protoc* **2013**, 1109-1114, doi:10.1101/pdb.top078782 (2013).

27 Turner, T. H., Alzubi, M. A. & Harrell, J. C. Identification of synergistic drug combinations using breast cancer patient-derived xenografts. *Sci Rep* **10**, 1493, doi:10.1038/s41598-020-58438-0 (2020).

28 Brancato, V. *et al.* 3D breast cancer microtissue reveals the role of tumor microenvironment on the transport and efficacy of free-doxorubicin in vitro. *Acta Biomater* **75**, 200-212, doi:10.1016/j.actbio.2018.05.055 (2018).

29 Hirschhaeuser, F. *et al.* Multicellular tumor spheroids: an underestimated tool is catching up again. *J Biotechnol* **148**, 3-15, doi:10.1016/j.jbiotec.2010.01.012 (2010).

30 Weeber, F., Ooft, S. N., Dijkstra, K. K. & Voest, E. E. Tumor Organoids as a Pre-clinical Cancer Model for Drug Discovery. *Cell Chem Biol* **24**, 1092-1100, doi:10.1016/j.chembiol.2017.06.012 (2017).

31 Yang, H., Sun, L., Liu, M. & Mao, Y. Patient-derived organoids: a promising model for personalized cancer treatment. *Gastroenterol Rep (Oxf)* **6**, 243-245, doi:10.1093/gastro/goy040 (2018).

32 Gendoo, D. M. A. *et al.* Whole genomes define concordance of matched primary, xenograft, and organoid models of pancreas cancer. *PLoS Comput Biol* **15**, e1006596, doi:10.1371/journal.pcbi.1006596 (2019).

33 Romero-Calvo, I. *et al.* Human Organoids Share Structural and Genetic Features with Primary Pancreatic Adenocarcinoma Tumors. *Mol Cancer Res* **17**, 70-83, doi:10.1158/1541-7786.MCR-18-0531 (2019).

34 Shi, J., Li, Y., Jia, R. & Fan, X. The fidelity of cancer cells in PDX models: Characteristics, mechanism and clinical significance. *Int J Cancer* **146**, 2078-2088, doi:10.1002/ijc.32662 (2020).

35 Dobrolecki, L. E. *et al.* Patient-derived xenograft (PDX) models in basic and translational breast cancer research. *Cancer Metastasis Rev* **35**, 547-573, doi:10.1007/s10555-016-9653-x (2016).

36 Wikswo, J. P. *et al.* Scaling and systems biology for integrating multiple organs-on-a-chip. *Lab Chip* **13**, 3496-3511, doi:10.1039/c3lc50243k

10.1039/c3lc50243k. (2013).

37 Becker, H. & Gärtner, C. Polymer microfabrication methods for microfluidic analytical applications. *Electrophoresis* **21**, 12-26, doi:10.1002/(SICI)1522-2683(20000101)21:1<12::AID-ELPS12>3.0.CO;2-7 (2000).

38 Tsai, H. F., Trubelja, A., Shen, A. Q. & Bao, G. Tumour-on-a-chip: microfluidic models of tumour morphology, growth and microenvironment. *J R Soc Interface* **14**, doi:10.1098/rsif.2017.0137 (2017).

39 Wang, H. F. *et al.* Tumor-Vasculature-on-a-Chip for Investigating Nanoparticle Extravasation and Tumor Accumulation. *ACS Nano* **12**, 11600-11609, doi:10.1021/acsnano.8b06846 (2018).

40 Pavesi, A. *et al.* A 3D microfluidic model for preclinical evaluation of TCR-engineered T cells against solid tumors. *JCI Insight* **2**, doi:10.1172/jci.insight.89762 (2017).

41 Kwak, B., Lee, Y., Lee, J., Lee, S. & Lim, J. Mass fabrication of uniform sized 3D tumor spheroid using high-throughput microfluidic system. *J Control Release* **275**, 201-207, doi:10.1016/j.jconrel.2018.02.029 (2018).

42 Subia, B. *et al.* Breast tumor-on-chip models: From disease modeling to personalized drug screening. *J Control Release* **331**, 103-120, doi:10.1016/j.jconrel.2020.12.057 (2021).

43 Eilenberger, C. *et al.* A Microfluidic Multisize Spheroid Array for Multiparametric Screening of Anticancer Drugs and Blood-Brain Barrier Transport Properties. *Adv Sci (Weinh)* **8**, e2004856, doi:10.1002/advs.202004856 (2021).

44 Benskey, M. J. & Manfredsson, F. P. Lentivirus Production and Purification. *Methods Mol Biol* **1382**, 107-114, doi:10.1007/978-1-4939-3271-9_8 (2016).

45 Pääkkö, M. *et al.* Enzymatic hydrolysis combined with mechanical shearing and high-pressure homogenization for nanoscale cellulose fibrils and strong gels. *Biomacromolecules* **8**, 1934-1941, doi:10.1021/bm061215p (2007).

46 Bhattacharya, M. *et al.* Nanofibrillar cellulose hydrogel promotes three-dimensional liver cell culture. *J Control Release* **164**, 291-298, doi:10.1016/j.jconrel.2012.06.039 (2012).

47 Moccia, C. & Haase, K. Engineering Breast Cancer On-chip-Moving Toward Subtype Specific Models. *Front Bioeng Biotechnol* **9**, 694218, doi:10.3389/fbioe.2021.694218 (2021).